DALTON
FULL PAPER

The spectroscopic, electrochemical and photophysical effects of the b_1/a_2 π* lowest unoccupied molecular orbital switching in $[M(CO)_4(N,N)]$ (M = Cr or W; N,N = 1,10-phenanthroline or 3,4,7,8-tetramethyl-1,10-phenanthroline). An experimental and DFT computational study †

Ian R. Farrell,[a] František Hartl,[b] Stanislav Záliš,[c] Taasje Mahabiersing[b] and Antonín Vlček, Jr.*[a,c]

[a] *Department of Chemistry, Queen Mary and Westfield College (University of London), London, UK E1 4NS. E-mail: a.vlcek@qmw.ac.uk*
[b] *Institute of Molecular Chemistry, Universiteit van Amsterdam, Nieuwe Achtergracht 166, 1018 WV Amsterdam, The Netherlands*
[c] *J. Heyrovský Institute of Physical Chemistry, Academy of Sciences of the Czech Republic, Dolejškova 3, CZ-182 23 Prague, Czech Republic*

Received 3rd July 2000, Accepted 26th September 2000
First published as an Advance Article on the web 16th November 2000

DFT calculations on the complexes $[M(CO)_4(N,N)]$ (M = Cr or W; N,N = 1,10-phenanthroline (phen) or 3,4,7,8-tetramethyl-1,10-phenanthroline (tmp)) have revealed that the phen and tmp complexes have different LUMOs: b_1 and a_2, respectively. Nevertheless, the character of the low-lying MLCT electronic transitions, calculated by time-dependent (TD) DFT, hardly changes on going from phen to tmp since the $b_1(d_{xz}) \longrightarrow b_1$(phen/tmp) transition is the strongest, whether the b_1(phen/tmp) orbital is the LUMO or not. The switching of LUMO orbitals is manifested by the following features exhibited by the tmp complexes, as compared with their phen counterparts: slightly lower IR ν(CO) frequencies, larger solvatochromism, higher relative resonance enhancement of the A_1^2 Raman ν(CO) peak and larger shifts of electrochemical reduction potentials from the "free" ligand value. The similar shapes and intensities of the visible absorption bands of the tmp and phen complexes and similarity of their resonance Raman spectra support the TD-DFT prediction of an essentially identical character of the electronic transition(s) responsible. Reduction of the $[M(CO)_4(N,N)]$ complexes produces the corresponding radical anions $[M(CO)_4(N,N)]^{\bullet -}$, which were characterized by EPR, IR and UV-Vis spectroelectrochemistry. In contrast with the neutral species, the properties of the radical-anionic tmp and phen complexes are very different due to difference between their SOMOs: a_2 and b_1, respectively. This is manifested by the profoundly different EPR hypefine splitting (hfs) patterns observed: $[M(CO)_4(phen)]^{\bullet -}$ complexes show large hfs from the ^{14}N donor atoms and from the pairs of ^{1}H atoms at C3,8 and C4,7 positions. On the other hand, EPR spectra of $[M(CO)_4(tmp)]^{\bullet -}$ show large hfs from ^{1}H atoms of a pair of CH_3 groups at C4,7 positions and two pairs of ^{1}H atoms at C2,9 and C5,6, while the ^{14}N splitting is rather small. Reasonable agreement between experimental and DFT-calculated hfs was obtained. The switching of LUMO character between b_1 and a_2 can have important implications for constructing molecular devices based on phen complexes.

Introduction

Transition-metal complexes of the polypyridine ligands 2,2′-bipyridine (bpy), 1,10-phenanthroline (phen) and their analogs continue to attract much research interest, especially because of their rich redox chemistry (electrochemistry) and photochemistry.[1,2] More recently, metal–polypyridine complexes have been used as active components in photo/redox active polynuclear and supramolecular assemblies, with possible future applications in molecular photonic and electronic devices.

To a large extent, the photo- and redox activity of polypyridine complexes is a consequence of the presence of empty polypyridine-localized π* orbitals which accept an electron upon reduction or metal-to-ligand charge transfer, MLCT, electronic excitation. The electrochemical, spectroscopic, photochemical, and photophysical behaviour of polypyridine complexes can broadly be tuned by varying the substituents located at various positions on bpy or phen rings.[2,3] In most cases, substituents affect the reduction potential, MLCT excited-state energies and lifetimes, as well as the energy gaps between MLCT states and photochemically or photophysically important ligand-field (LF) and intra-ligand (IL) states by changing the π* (LUMO) orbital energy. More drastic variations in polypyridine structure also affect the localization of the π* (LUMO) at N donor atoms, whereby metal–ligand π delocalization is influenced.[1,2,4–6] This happens either on introduction of more N atoms into the polypyridine rings (*i.e.* for polyazine ligands) or on replacing polypyridines with other α-diimines, *e.g.* for 1,4-diazabutadienes.[1] Nevertheless, the π* LUMO in all of these ligands has the same general nature and the same b_1 symmetry, which is suitable for a π overlap with the metal d_{xz} orbital of the metal atom, Fig. 1.

In this respect, phen-type ligands are rather exceptional, since they have two empty π* orbitals of b_1 and a_2 symmetry, which are very close in energy. The π* orbital ordering in phen itself had been a subject of some controversy until an EPR study demonstrated that the phen$^{\bullet -}$ radical anion has a $^2B_1$ ground state, indicating the b_1 symmetry of the phen LUMO.[7]

† Electronic supplementary information (ESI) available: selected DFT calculated and experimental bond lengths and angles; IR and UV-Vis spectra for spectroelectrochemical reductions. See http://www.rsc.org/suppdata/dt/b0/b005279p/

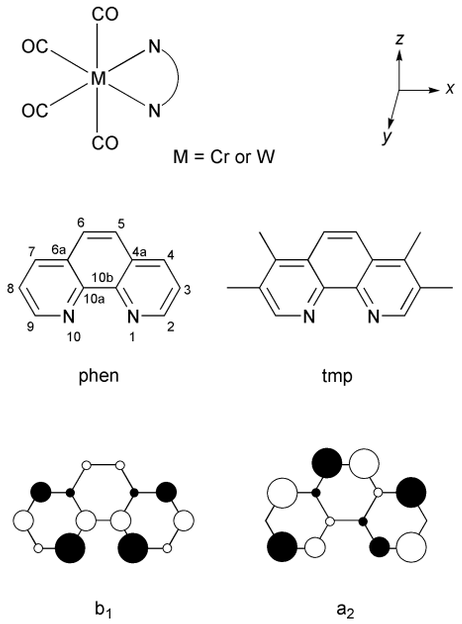

Fig. 1 Schematic structures of $[M(CO)_4(N,N)]$ complexes, phen and tmp ligands, and the chosen orientation of axes. Bottom: qualitative pictures of b_1 and a_2 lowest unoccupied MOs.[8,9]

Introduction of methyl groups into the 4 and 7 positions alone does not affect the energetic ordering of the lowest unoccupied orbitals.[7,8] However, EPR[8,9] and *ab initio* theoretical[9] studies of the "free" ligands have demonstrated that a "LUMO switching" occurs on going from phen or 4,7-Me_2-phen to 3,4,7,8-Me_4-phen (tmp), whose radical anion has a $^2A_2$ ground state, characterized by low a(N) hyperfine splitting constant. Amongst metal–phenanthroline complexes, b_1/a_2 orbital switching has been indicated[8] for reduced $[Pt(N,N)(mes)_2]^{\bullet -}$ complexes; N,N = phen, 4,7-Me_2-phen or tmp; mes = mesityl = $C_6H_2Me_3$-2,4,6. However, the evidence was only indirect, since the hyperfine splitting due to ligand N and H atoms was not observed. Nevertheless, a much lower platinum splitting constant, higher g_{iso} value and a lower g anisotropy observed for N,N = tmp all point to a $^2A_2$ state.[8] These features stem from a much weaker π interaction between the metal d(π) orbitals and the a_2 LUMO, as compared with the b_1 orbital. This is the consequence of a much lower participation of the $2p_z$(N) orbitals in the a_2 π* orbital and its orthogonality to the d_{xz} metal orbital.[9]

The possibility to control the extent of π interaction between the metal and phen ligand by orbital switching could be of importance in the development of molecular devices. However, it is first necessary to demonstrate that this effect is more general in co-ordination and organometallic phen-type complexes and to understand its photophysical and photochemical implications. To this end, we have investigated the spectroscopic (UV-Vis absorption, resonance Raman), electrochemical, spectroelectrochemical (EPR, IR, UV-Vis), and emission properties of the complexes $[M(CO)_4(N,N)]$; M = Cr or W; N,N = phen or tmp. Group 6 tetracarbonyls are excellent models for such a study because of their structural simplicity and the presence of CO ligands, whose IR and resonance Raman bands are sensitive markers for electron density distribution.

A better understanding of the redox and spectroscopic properties of phen complexes is now becoming more important because of their increasing use as photocatalysts,[10,11] building blocks of molecular dyads,[12,13] supramolecules,[14–17] especially catenanes and rotaxanes, light-harvesting molecular assemblies,[18] molecular wires or switches[19] and DNA intercalators.[20,21] Notably, the phen ligand and its derivatives show several specific features which can have significant photochemical, photophysical or electrochemical consequences. These include, for example, energetically low-lying ππ* intraligand excited states[4,22–24] and an exceptional ability of 2,9-substituted phen to form tetrahedral copper(I) complexes with long-lived MLCT states and stable one- or two-electron reduction products.[14,25] The substituent-induced switching of the b_1/a_2 energy ordering could be another important factor controlling properties of 1,10-phenanthroline and its transition metal complexes.[8,9]

Experimental

Ground state electronic structure calculations of $[M(CO)_4(phen)]$ and $[M(CO)_4(tmp)]$ complexes have been performed with density functional theory (DFT) using the ADF1999 software package.[26,27] The lowest excited states of the closed shell complexes were calculated using the time-dependent DFT method (TD-DFT), employing the ADF-RESPONSE program.[28] The calculations were performed under C_{2v} constrained symmetry, the x axis being coincident with the C_2 symmetry axis. The N,N ligand and equatorial CO ligands are located in the xy plane and axial CO ligands lie on the z axis, Fig. 1.

Slater type orbital (STO) double-ζ basis sets were used for H atoms. Triple-ζ quality basis sets with polarization functions were employed for all other atoms. Inner shells were represented by a frozen core approximation (1s for C, N and O; 1s–3p for Cr and 1s–4d for W were kept frozen). The following density functionals were used: local density approximation (LDA) with Vosko–Wilk–Nusair (VWN) parametrization of electron gas data or functionals including Becke's gradient correction[29] to the local exchange expression in conjunction with Perdew's gradient correction[30] to the LDA expression (BP). A scalar relativistic (SR) zero order regular approximation (ZORA) was used. The adiabatic local density approximation (ALDA) with the frequency dependence ignored was employed in post-SCF time dependent DFT calculations.

Materials

All chemicals were of analytical purity (Aldrich or Strem). Solvents were dried and degassed using standard procedures. Sample manipulation and all measurements were performed under a nitrogen or argon atmosphere using Schlenk techniques. The complexes $[M(CO)_4(N,N)]$ were synthesized by a modified literature method[31] which involved refluxing 4.9 mmol of $M(CO)_6$ (*i.e.* 1.08 g of $Cr(CO)_6$ or 1.72 g of $W(CO)_6$) and 4.5 mmol of the N,N ligand (*i.e.* 0.81 g of phen or 1.06 g of tmp) in 80 mL of toluene (M = Cr) or xylene (M = W) for 4 h. Scarlet-red crystals of the product precipitated during the reaction and were isolated by filtration. This crude material was recrystallised from dichloromethane solution by the addition of iso-octane followed by the removal of approximately 75% of the chlorinated solvent by distillation. On subsequent refrigeration red crystals of $[M(CO)_4(N,N)]$ formed in approximately 80% yield. In solution the complexes are sensitive towards air and light. The products were characterized by FT-IR (in CH_2Cl_2 and *n*PrCN) and ^{1}H NMR (in CD_2Cl_2) spectra which have proven the sample purity and identity. Spectral data obtained on known phen complexes agree with those reported in the literature. Newly made tmp complexes were characterised by comparison of their IR and NMR spectra with those of their known phen congeners. In addition, MS-FD$^+$ was used to confirm the composition and purity of the tmp complexes. This procedure was used instead of elemental analysis which is often less reliable for this type of compound.

$[Cr(CO)_4(phen)]$: ^{1}H NMR $\delta = 9.50$ (dd, 2H, H^2), 8.39 (dd, 2H, H^4), 7.93 (s, 2H, H^5) and 7.81 (dd, 2H, H^3, $J(H^2H^3) = 5.07$, $J(H^2H^4) = 1.16$, $J(H^3H^4) = 8.31$ Hz). $[Cr(CO)_4(tmp)]$: ^{1}H NMR δ 9.21 (s, 2H, H^2), 8.08 (s, 2H, H^5), 2.71 (s, 6H, *p*-CH_3) and 2.55 (s, 6H, *m*-CH_3); MS-FD$^+$ *m*/*z* 400 [M$^+$]. $[W(CO)_4(phen)]$: ^{1}H NMR: δ 9.54 (dd, 2H, H^2), 8.48 (dd, 2H, H^4), 7.99 (s, 2H,

Table 1 Infrared absorption bands of $[M(CO)_4(N,N)]$ complexes (M = Cr or W; N,N = phen or tmp) and their anions in the ν(CO) region. Data in cm^{-1}. Measured in *n*PrCB at room temperature. Δ = shift on reduction

	Cr(phen)	$Cr(phen)^{\bullet -}$	Δ	W(phen)	$W(phen)^{\bullet -}$	Δ
A_1^2	2008	1988	−20	2006	1983	−23
B_1	1901	1871	−30	1892	1857	−35
A_1^1	1881	1849	−32	1875	1835	−40
B_2	1833	1798	−35	1831	1793	−38
	Cr(tmp)	$Cr(tmp)^{\bullet -}$	Δ	W(tmp)	$W(tmp)^{\bullet -}$	Δ
A_1^2	2006	1988	−18	2004	1983	−21
B_1	1896	1871	−25	1887	1856	−31
A_1^1	1876	1847	−29	1868	1838	−30
B_2	1830	1797	−33	1827	1792	−35

H^5) and 7.77 (dd, 2H, H^3, $J(H^2H^3) = 5.20$, $J(H^2H^4) = 1.15$, $J(H^3H^4 = 8.22$ Hz). $[W(CO)_4(tmp)]$: ^1H NMR: δ 9.25 (s, 2H, H^2), 8.14 (s, 2H, H^5), 2.75 (s, 6H, *p*-CH_3) and 2.57 (s, 6H, *m*-CH_3); MS-FD^+ *m*/*z* 532 $[M^+]$.

Instrumentation

UV-Vis absorption spectra were recorded on a Hewlett-Packard 6453 diode array spectrophotometer, NMR spectra on a Bruker AM 250 MHz spectrometer. Time-resolved emission spectra were recorded from optically dilute solutions of $[W(CO)_4(N,N)]$ (10^{-5} M) excited using a Quanta Ray PDL3 dye laser pumped by the 355 nm line of a Spectra Physics Nd:YAG laser. Emitted light was detected and analysed with an EG&G OMA III instrument. Resonance Raman spectra were obtained from tungsten complexes using a Dilor XY spectrometer with a Spectra Physics 2016 Ar^+ laser. Samples were prepared as CH_2Cl_2 solutions and placed in a rotating cell. Cyclic voltammograms were measured from $(1–2) \times 10^{-3}$ M solutions in either THF or *n*PrCN containing 0.1 M tBu_4NBF_4 that was dried by heating under vacuum at 100 °C overnight. Ferrocene (Fc) was added to sample solutions as an internal potential reference and a standard to assess electrochemical reversibility.[32] An EG&G PAR 283 potentiostat, 0.5 mm diameter platinum disk working electrode, platinum wire auxiliary electrode and silver wire pseudoreference electrode were used. IR spectra were recorded using a Bio-Rad FTS-7 spectrometer (16 scans, 2 cm^{-1} resolution). Both infrared and UV-vis absorption spectra of reduction products in *n*PrCN at room temperature were recorded spectroelectrochemically using controlled-potential electrolysis in an OTTLE cell[33] that was equipped with a platinum mini-grid working electrode consisting of 32 wires per centimeter and CaF_2 optical windows. A PA4 potentiostat (EKOM, Czech Republic) was used as a power supply. Solutions consisted of approximately 0.1 M tBu_4NBF_4 and between 10^{-2} and 10^{-3} M $[M(CO)_4(N,N)]$ complex. EPR spectroelectrochemistry was performed using a Varian Century E-104A X-band spectrometer. Radical anions were produced electrochemically (PA4) in a custom built three electrode (silver pseudoreference, platinum auxiliary and gold working) EPR cell.[34] Sample concentrations were typically around 10^{-3} M in THF containing *ca*. 0.1 M tBu_4NBF_4 electrolyte. EPR spectra were simulated using WinSim software version 0.96 distributed by the US National Institute of Environmental Health Services (http://epr.niehs.nih.gov/).

Results

Ground state structures

All the phen and tmp complexes investigated herein give very similar infrared spectra in the ν(CO) region which are characteristic of *cis*-tetracarbonyl complexes.[35–41] see Table 1 and the ESI. The ν(CO) bands were assigned by analogy with the EFFF normal co-ordinate analysis of $[Cr(CO)_4(bpy)]$.[40,41]

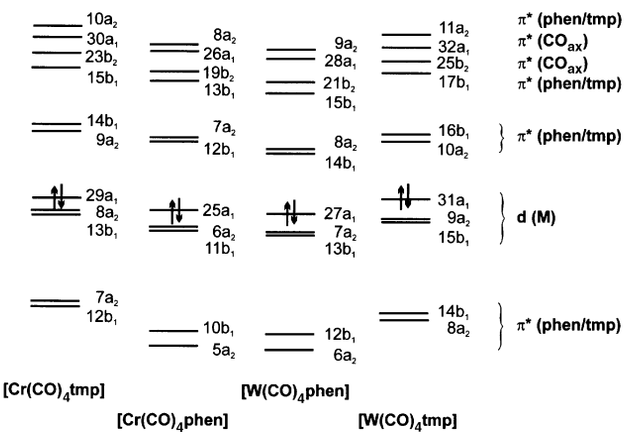

Fig. 2 Qualitative molecular orbital diagrams of $[M(CO)_4(N,N)]$ complexes (M = Cr or W; N,N = phen or tmp).

Calculated (optimized) bond lengths and angles (see ESI) of all four complexes are very similar, also to those calculated previously[42] for $[Cr(CO)_4(bpy)]$. They compare well with the values determined for $[Cr(CO)_4(phen)]$ and $[W(CO)_4(phen)]$ by X-ray diffraction.[43–45] The phen or tmp ligand lies in the equatorial (*x*,*y*) molecular plane. The N–M–N bite angle is rather small, 72–77°. Internal bond lengths of the N,N ligands are very similar for phen and tmp. Only the C2–C3, C3–C4, and C4–C4a bonds are slightly longer (by 0.008–0.013 Å) for tmp, presumably due to steric effects of the Me groups. Ligand structures are almost independent of the metal, Cr or W. On going from phen to tmp, the calculated M–N bond lengths elongate by 0.042 Å for Cr and by 0.020 Å for W. This could be caused by a weaker π-back donation to the less electron-accepting tmp ligand. The axial OC–M–CO moiety is nearly linear, the axial CO ligands being slightly bent away from the phen/tmp ligand: the calculated $(OC)_{ax}$–M–$(CO)_{ax}$ angles range from 170.6 to 173.5°, in a good agreement with experimental values of 168.9–172.4°.

Table 2 summarizes the calculated energies and characters of the frontier molecular orbitals of $[Cr(CO)_4(phen)]$ and $[W(CO)_4(phen)]$. Orbital characters obtained for the corresponding tmp complexes are very similar, as is demonstrated in Table 2 for $[W(CO)_4(tmp)]$. MO diagrams and numbering of relevant molecular orbitals are shown in Fig. 2. The three highest occupied molecular orbitals are very close in energy. Hereinafter, they will be denoted a_1(HOMO), a_2(HOMO) and b_1(HOMO). They are predominantly d orbitals with a significant admixture of a π*(CO) character. A phen π/π* character contributes 14 and 17% to the $11b_1$(Cr) and $13b_1$(W) HOMOs, respectively.

The lowest unoccupied molecular orbital (LUMO) of $[W(CO)_4(phen)]$ and $[Cr(CO)_4(phen)]$ was calculated as having

Table 2 ADF/BP calculated one-electron energies and percentage composition of selected highest occupied and lowest unoccupied molecular orbitals of $[M(CO)_4(N,N)]$ complexes (M = Cr or W; N,N = phen or tmp) expressed in terms of the constituent fragments (%)

$[Cr(CO)_4(phen)]$						
MO	*E*/eV	Character	Cr	$(CO)_{ax}$	$(CO)_{eq}$	phen
Unoccupied						
$8a_2$	−1.53	π* phen			1	98
$26a_1$	−1.58	CO_{ax}	4 (s); 6(p_x); 8(d)	78	1	3
$19b_2$	−1.84	CO_{ax}	11(p_y)	73	11	4
$13b_1$	−2.21	π* phen		1		98
$7a_2$	−3.36	π* phen				99
$12b_1$	−3.37	π* phen		4	2	90
Occupied						
$25a_1$	−4.71	d + CO_{eq}	2 (p_x); 63 (d)	1	33	
$6a_2$	−4.96	d + CO	58 (d_{yz})	22	15	4
$11b_1$	−4.99	d + CO	54 (d_{xz})	22	9	14
$10b_1$	−6.82	π phen	1 (d_{xz})	1		98
$5a_2$	−7.12	π phen				99
$[W(CO)_4(phen)]$						
MO	*E*/eV	Character	W	$(CO)_{ax}$	$(CO)_{eq}$	phen
Unoccupied						
$9a_2$	−1.73	π* phen			2	97
$28a_1$	−1.78	CO_{ax}	2 (s); 8(p_x); 2(d)	88		
$21b_2$	−2.02	CO_{ax}	11(p_y)	73	11	4
$15b_1$	−2.34	π* phen				99
$8a_2$	−3.49	π* phen				99
$14b_1$	−3.55	π* phen	4(d_{xz}); 1(p_z)	4	4	87
Occupied						
$27a_1$	−4.70	d + CO_{eq}	58(d)	1	38	1
$7a_2$	−5.02	d + CO	54 (d_{yz})	25	16	5
$13b_1$	−5.11	d + CO	50 (d_{xz})	22	11	17
$12b_1$	−6.98	π phen	1 (d_{xz})	1		98
$6a_2$	−7.27	π phen				99
Comparison of $[W(CO)_4(phen)]$ and $[W(CO)_4(tmp)]$						
MO	*E*/eV	Character	W	$(CO)_{ax}$	$(CO)_{eq}$	phen
L = phen						
$8a_2$	−3.49	π* phen	0.27 (d)	0.31	0.47	98.9
$14b_1$	−3.55	π* phen	4.43(d_{xz}); 0.51(p_z)	4.47	3.78	86.93
$13b_1$	−5.11	d + CO	49.8(d_{xz})	22.5	11	17.5
L = tmp						tmp
$16b_1$	−3.18	π* phen	3.38(d_{xz}); 0.53(p_z)	4.40	2.93	88.87
$10a_2$	−3.31	π* phen	0.21 (d)	0.24	0.37	99.11
$15b_1$	−4.46	d + CO	50.5 (d_{xz})	22.3	12.5	15.5

b_1 symmetry and a predominant (87–90%) phen π* character. The d_{xz} orbital contributes 4%. The second unoccupied MO (abbreviated LUMO + 1) is a phen-localized π* orbital of a_2 symmetry: $7a_2$ in $[Cr(CO)_4(phen)]$ and $8a_2$ in $[W(CO)_4(phen)]$. The calculated energy difference between b_1 LUMO and a_2 LUMO + 1 is rather small, 0.01 eV for Cr and 0.06 eV for W. Importantly, switching of the energy order of the lowest unoccupied b_1 and a_2 orbitals was calculated to occur on going from phen to tmp complexes: The $9a_2$ and $10a_2$ tmp-localized orbitals were calculated to be the LUMOs of $[Cr(CO)_4(tmp)]$ and $[W(CO)_4(tmp)]$, respectively. The corresponding a_2 orbital energies are −3.15 eV for $[Cr(CO)_4(tmp)]$ and −3.31 eV for $[W(CO)_4(tmp)]$. The $14b_1$ orbital of $[Cr(CO)_4(tmp)]$ and the $16b_1$ orbital of $[W(CO)_4(tmp)]$ are LUMO + 1, occurring at −2.97 and −3.18 eV, respectively. The shapes of the a_2 and b_1 lowest unoccupied orbitals are compared in Fig. 3. The b_1(LUMO) is π-antibonding towards N–C2, N–C10b, C3–C4, and C4a–C10b bonds, and π-bonding with respect to C4–C4a and C10a–C10b bonds and their symmetric counterparts. Its localization on the C5 and C6 atoms is negligible. Fig. 3 also shows the involvement of equatorial π*(CO) and axial σ(OC–M–CO) orbitals in the b_1(LUMO). By contrast, the lowest unoccupied a_2 is 99% ligand-localized, the contribution from the $M(CO)_4$ fragment being negligible for symmetry reasons. The a_2 orbital is π-antibonding with respect to N–C2, C4–C4a, C5–C6 and C10a–C10b bonds. It is π-bonding toward N–C10a and C4a–C5 bonds. The a_2 orbital is virtually absent at C3 and C8 atoms while it is heavily localized at C5 and C6 positions.

Electronic absorption and resonance Raman spectra

All four complexes show a broad absorption band in the visible spectral region with a prominent shoulder on its high-energy side, see Fig. 4. The experimental and TD-DFT theoretical data are summarized in Tables 3 and 4, respectively. The molar

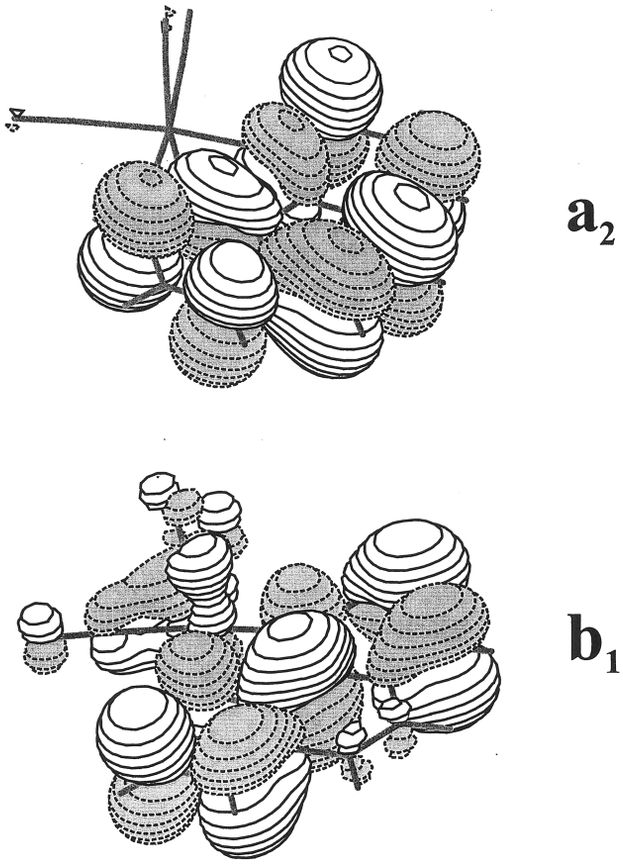

Fig. 3 DFT-calculated shapes of a_2 (top) and b_1 (bottom) lowest unoccupied orbitals of $[W(CO)_4(phen)]$. Virtually identical orbital shapes were obtained for other complexes studied herein.

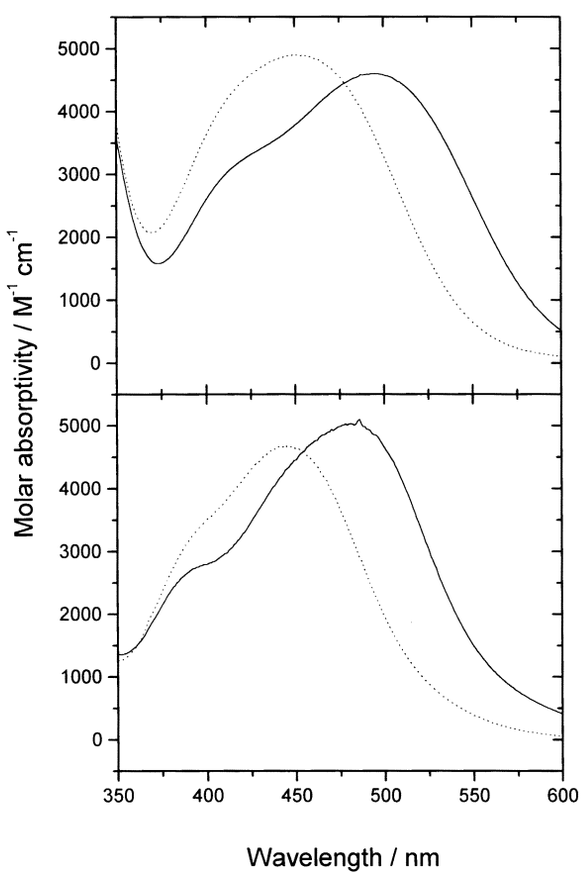

Fig. 4 UV-Vis absorption spectra of $[Cr(CO)_4(phen)]$ (top, full); $[Cr(CO)_4(tmp)]$ (top, dashed); $[W(CO)_4(phen)]$ (bottom, full) and $[W(CO)_4(tmp)]$ (bottom, dashed). Measured in CH_2Cl_2.

Table 3 Visible absorption spectra of $[M(CO)_4(N,N)]$ complexes (M = Cr or W; N,N = phen or tmp)

Compound	Solvent	λ_{max}/ nm	E_{max}/ eV	ΔE_{max}[a]/ cm^{-1}
$[Cr(CO)_4(phen)]$	CH_2Cl_2	495	2.50	1044
	Toluene	522	2.38	
$[Cr(CO)_4(tmp)]$	CH_2Cl_2	453	2.74	1498
	Toluene	486	2.55	
$[W(CO)_4(phen)]$	CH_2Cl_2	486	2.55	1120
	Toluene	514	2.41	
$[W(CO)_4(tmp)]$	CH_2Cl_2	445	2.79	1551
	Toluene	478	2.59	

[a] Solvatochromism: $\Delta E_{max} = E_{max}(CH_2Cl_2) - E_{max}(toluene)$.

absorptivity and solvatochromism of the visible absorption band, as well as its blue shift on going from phen to tmp, are characteristic of the allowed $b_1(HOMO) \longrightarrow b_1(N,N)$ MLCT transition to the b^1A_1 state.[1,46,47] Indeed, TD-DFT calculations have identified the corresponding $a^1A_1 \longrightarrow b^1A_1$ transition to be the main contributor to the lowest absorption band for all four complexes. In the case of $[Cr(CO)_4(phen)]$ and $[W(CO)_4(phen)]$ this transition combines 86% $b_1(HOMO) \longrightarrow b_1(LUMO)$ and 7% $a_2(HOMO) \longrightarrow a_2(LUMO + 1)$ orbital excitations. For $[Cr(CO)_4(tmp)]$ and $[W(CO)_4(tmp)]$ the $a^1A \longrightarrow b^1A$ transition is over 90% $b_1(HOMO) \longrightarrow b_1(LUMO + 1)$ in character. In addition, a 6–7 times weaker transition to the b^1B_2 state (a^1B_2 for $[Cr(CO)_4(tmp)]$) contributes to the low-energy side of the broad visible band, see Table 4. Finally, a transition whose main component involves excitation from $b_1(HOMO)$ to the $b_1(LUMO + 2)$ π^* phen/tmp orbital is probably responsible for the broadening of the high-energy side of the visible absorption band. For tungsten complexes this transition also contains a contribution from a $W \longrightarrow CO$ MLCT transition.

The agreement between TD-DFT calculated and experimental values is reasonable. TD-DFT correctly reproduces the experimentally observed intensity increase of the $a^1A_1 \longrightarrow b^1A_1$ MLCT transition on going from Cr to W and from $[W(CO)_4(phen)]$ to $[W(CO)_4(tmp)]$. Calculated transition energies are smaller than those observed experimentally by 0.33–0.51 eV, presumably due to the neglect of medium effects. The same reason is probably responsible for the smaller calculated blue shift between phen and tmp tungsten complexes than that measured experimentally.

A well resolved shoulder occurs at *ca.* 420 and 400 nm for the complexes of Cr and W respectively, regardless of the N,N ligand; phen or tmp. A very similar shoulder was observed in the spectra of many other $[M(CO)_4(\alpha\text{-diimine})]$ complexes, as well as $[W(CO)_4(en)]$.[1,46,48–52] Owing to a lack of solvatochromism, this band is traditionally attributed to a LF transition. However, our TD-DFT calculations found the lowest LF transition of $[Cr(CO)_4(phen)]$ and $[W(CO)_4(phen)]$ at 4.88 eV (254 nm) and 5.08 eV (244 nm), respectively. This excludes the LF origin of the 400–420 nm shoulder. Instead, its assignment to M→CO MLCT transitions seems more appropriate, both in the view of the TD-DFT calculations (Table 4) and previous results[53,54] on $M(CO)_6$. The calculated transitions are rather weak but may gain intensity by mixing with MLCT transitions to the higher $b_1(LUMO + 2)$ π^* orbital of the N,N ligand, as is indicated by TD-DFT for $[W(CO)_4(phen)]$ and $[W(CO)_4(tmp)]$. On the other hand, TD-DFT provides no evidence for a mixing between these M→CO MLCT states and LF states, since the low-lying $\pi^*(CO)$ orbitals have only negligible contributions from metal d orbitals, see Table 2.

Resonance Raman spectra (Fig. 5) were measured for $[W(CO)_4(phen)]$ and $[W(CO)_4(tmp)]$ in CH_2Cl_2 solution, using 514.5 and 488 nm excitation directed into the main absorption band. Intensity enhancement is larger when 488 nm excitation

Table 4 TD-DFT calculated singlet excitation energies (eV) for $[M(CO)_4(N,N)]$ complexes (M = Cr or W; N,N = phen or tmp). The most important contributor to the visible absorption band is shown in bold. Transitions with very small oscillator strengths are omitted

State	Composition[a]	ΔE[b]/eV	f[c]	Character[d]
$[Cr(CO)_4(phen)]$				
a^1B_2	94% ($6a_2 \longrightarrow 12b_1$)	1.63	0.0001	MLCT(phen)
b^1B_2	93% ($11b_1 \longrightarrow 7a_2$)	1.76	0.017	MLCT(phen)
b^1A_1	**86% ($11b_1 \longrightarrow 12b_1$), 7% ($6a_2 \longrightarrow 7a_2$)**	**2.05**	**0.096**	**MLCT(phen)**
c^1B_2	94% ($6a_2 \longrightarrow 13b_1$)	2.77	0.003	MLCT(phen)
c^1A_1	93% ($11b_1 \longrightarrow 13b_1$)	2.93	0.043	MLCT(phen)
d^1B_2	96% ($25a_1 \longrightarrow 19b_2$)	2.99	0.004	MLCT(CO)
a^1B_1	62% ($6a_2 \longrightarrow 19b_2$), 28% ($11b_1 \longrightarrow 26a_1$)	3.37	0.003	MLCT(CO)
d^1A_1	93% ($6a_2 \longrightarrow 8a_2$)	3.48	0.066	MLCT(phen)
e^1A_1	72% ($5a_2 \longrightarrow 7a_2$), 15% ($11b_1 \longrightarrow 13b_1$)	4.19	0.064	IL + MLCT(phen)
$[Cr(CO)_4(tmp)]$				
a^1B_2	95% ($13b_1 \longrightarrow 9a_2$)	1.65	0.014	MLCT(tmp)
b^1B_2	95% ($8a_2 \longrightarrow 14b_1$)	1.77	0.005	MLCT(tmp)
b^1A_1	**92%($13b_1 \longrightarrow 14b_1$)**	**2.09**	**0.100**	**MLCT(tmp)**
c^1B_2	98% ($8a_2 \longrightarrow 15b_1$)	2.83	0.002	MLCT(tmp)
c^1A_1	95% ($13b_1 \longrightarrow 15b_1$)	2.95	0.043	MLCT(tmp)
d^1B_2	95% ($29a_1 \longrightarrow 23b_2$)	2.96	0.005	MLCT(CO)
a^1B_1	74% ($8a_2 \longrightarrow 23b_2$), 26% ($13b_1 \longrightarrow 30a_1$)	3.29	0.003	MLCT(CO)
d^1A_1	70% ($8a_2 \longrightarrow 10a_2$), 16% ($12b_1 \longrightarrow 14b_1$)	3.62	0.053	MLCT(tmp)
e^1A_1	51% ($12b_1 \longrightarrow 14b_1$), 37% ($7a_2 \longrightarrow 9a_2$)	4.00	0.094	IL
$[W(CO)_4(phen)]$				
a^1B_2	94% ($7a_2 \longrightarrow 14b_1$)	1.53	0.0007	MLCT(phen)
b^1B_2	94% ($13b_1 \longrightarrow 8a_2$)	1.77	0.019	MLCT(phen)
b^1A_1	**86% ($13b_1 \longrightarrow 14b_1$), 7% ($7a_2 \longrightarrow 8a_2$)**	**2.05**	**0.124**	**MLCT(phen)**
c^1B_2	94% ($7a_2 \longrightarrow 15b_1$)	2.70	0.003	MLCT(phen)
d^1B_2	93% ($27a_1 \longrightarrow 21b_2$)	2.80	0.005	MLCT(CO)
c^1A_1	87% ($13b_1 \longrightarrow 15b_1$), 5% ($27a_1 \longrightarrow 28a_1$)	2.91	0.043	MLCT(phen, CO)
a^1B_1	62% ($7a_2 \longrightarrow 21b_2$), 37% ($13b_1 \longrightarrow 28a_1$)	3.27	0.004	MLCT(CO)
d^1A_1	93% ($7a_2 \longrightarrow 9a_2$)	3.43	0.103	MLCT(phen)
e^1A_1	72% ($6a_2 \longrightarrow 8a_2$), 15% ($12b_1 \longrightarrow 15b_1$)	4.19	0.064	IL
$[W(CO)_4(tmp)]$				
a^1B_2	52% ($9a_2 \longrightarrow 16b_1$), 48% ($15b_1 \longrightarrow 10a_2$)	1.62	0.004	MLCT(tmp)
b^1B_2	48% ($9a_2 \longrightarrow 16b_1$), 50% ($15b_1 \longrightarrow 10a_2$)	1.68	0.019	MLCT(tmp)
b^1A_1	**91% ($15b_1 \longrightarrow 16b_1$)**	**2.08**	**0.131**	**MLCT(tmp)**
c^1B_2	60% ($31a_1 \longrightarrow 25b_2$), 36% ($9a_2 \longrightarrow 17b_1$)	2.78	0.007	MLCT(CO, tmp)
c^1A_1	83% ($15b_1 \longrightarrow 17b_1$), 12% ($31a_1 \longrightarrow 32a_1$)	2.92	0.042	MLCT(tmp, CO)
a^1B_1	63% ($9a_2 \longrightarrow 25b_2$), 36% ($15b_1 \longrightarrow 32a_1$)	3.24	0.003	MLCT(CO)
d^1A_1	78% ($9a_2 \longrightarrow 11a_2$), 11% ($8a_2 \longrightarrow 10a_2$)	3.52	0.048	MLCT(tmp)
e^1A_1	44% ($8a_2 \longrightarrow 10a_2$), 43% ($14b_1 \longrightarrow 16b_1$)	3.98	0.092	A + IL

[a] Compositions of electronic transitions are expressed in terms of contributing excitation between ground-state Kohn–Sham molecular orbitals, see Table 2 and Fig. 2. [b] Transition energy from the a^1A_1 ground state. [c] Oscillator strength. [d] The ligand in parentheses denotes the direction of MLCT transitions; IL = intraligand transition.

is employed. Spectra of both complexes show a group of weak bands between 430 and 570 cm^{-1} due to ν(CrC) and δ(CrCO) skeletal vibrations,[41] a set of phen/tmp-localized vibrations between 1100 and 1650 cm^{-1} and a peak at *ca.* 2006 cm^{-1} due to the in-phase A_1^2 ν(CO) vibration.[41] The overall Raman spectral pattern and shifts are very similar for $[W(CO)_4(phen)]$ and $[W(CO)_4(tmp)]$. The only major difference occurs for the highest intraligand vibrations which are rather strong for phen (1579, 1629 cm^{-1}) but very weak for tmp (1566, 1592 cm^{-1}). The Raman shift values of the phen-localized vibrations are similar to those reported[55] for $[Ru(phen)_3]^{2+}$.

The relative enhancement of the ν(CO) Raman peak with respect to the most intense peaks due to phen and tmp vibrations increases on going from 514.5 to 488 nm excitation. It is also higher for tmp than for phen: For $[W(CO)_4(phen)]$ the intensity ratios between the ν(CO) peak and those at 1449 and 1513 cm^{-1} increase from the respective values of 1.0 and 1.2 to 1.3 and 1.6:1, respectively, on changing the excitation wavelength from 514.5 to 488 nm. For $[W(CO)_4(tmp)]$ the intensity ratios between the ν(CO) peak and those at 1445 and 1520 cm^{-1} increase from 1.3 and 1.6:1 at 514.5 nm to 2.0 and 1.7:1 at 488 nm. Overall, the high resonance enhancements of the Raman peaks corresponding to A_1^2 ν(CO) and intraligand vibrations point to a highly localized $W(CO)_4 \rightarrow N,N$ MLCT character of the resonant electronic transition for both complexes.[1,46,47]

Time-resolved luminescence

$[W(CO)_4(phen)]$ and $[W(CO)_4(tmp)]$ in a 2-MeTHF glass at 80 K show broad, unstructured emission bands at *ca.* 648 and 608 nm, respectively, when excited at 440 nm. A very weak and broad emission band was also observed in fluid toluene solution at *ca.* 680 and 730 nm for phen and tmp, respectively. Based on the band shape, energy and rigidochromism, this emission is attributed to low-lying spin-triplet MLCT state(s). The emission decay at 80 K follows double-exponential kinetics with lifetimes of 612 ± 21, 2684 ± 93 ns for $[W(CO)_4(tmp)]$ and 150 ± 4, 487 ± 18 ns for $[W(CO)_4(phen)]$. The increase in lifetime on going from phen to tmp is in accordance with the energy gap law, since there is a rise in emission energy of 1015

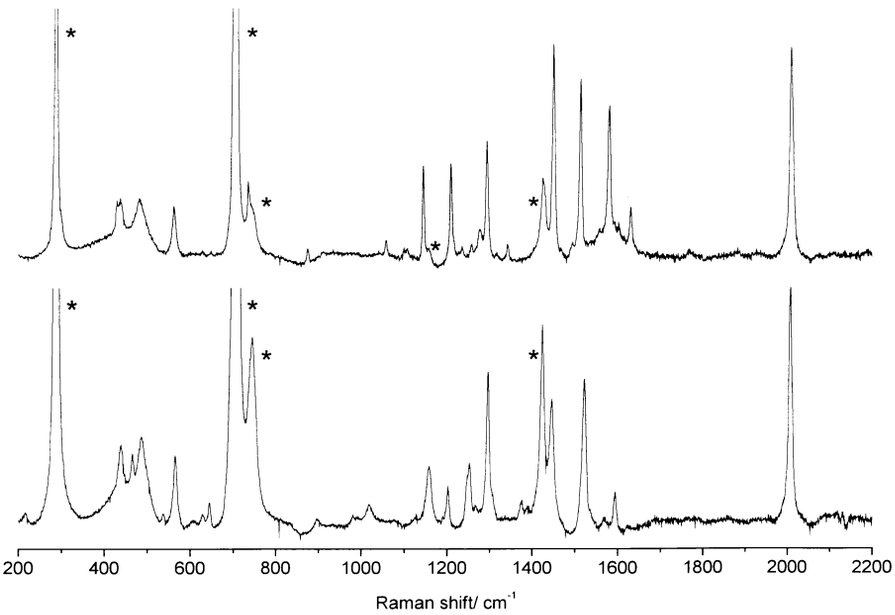

Fig. 5 Resonance Raman spectra of $[W(CO)_4(phen)]$ (top) and $[W(CO)_4(tmp)]$ (bottom) measured in CH_2Cl_2, excited at 514.5 nm. *: Solvent peaks. Principal peaks occur at 433, 484, 560, 1143, 1207, 1293, 1449, 1512, 1579, 1629 and 2007 cm^{-1} for $[W(CO)_4(phen)]$ and at 437, 464, 487, 565, 1158, 1200, 1251, 1295, 1444, 1521, 1566vw, 1592vw and 2006 cm^{-1} for $[W(CO)_4(tmp)]$.

cm^{-1}. However, the 4–5 fold effect is too large to be accounted for solely by this phenomenon. Apparently, it is, in part, caused by the different contributions of individual orbital excitations to the excited states involved.

Reduction: electrochemistry and spectroelectrochemistry

Cyclic voltammetry. The $[M(CO)_4(N,N)]$ (M = Cr or W; N,N = phen or tmp) complexes undergo a one-electron reduction that is both chemically and electrochemically reversible at modest scan rates in *n*PrCN or THF solutions at room temperature. This reversibility shows that stable radical anions $[M(CO)_4(N,N)]^{\bullet -}$ are produced. The corresponding half-wave potentials measured in *n*PrCN *vs.* $Fc–Fc^+$ are: −2.04 (Cr/phen), −2.21 (Cr/tmp), −1.87 (W/phen), and −2.09 V (W/tmp). The potentials measured in THF are more negative by 60–80 mV. Two more chemically irreversible reduction steps were observed at more negative potentials.

IR spectroelectrochemistry. IR spectra of the $[M(CO)_4(N,N)]^{\bullet -}$ radical anions were measured in an OTTLE cell upon controlled-potential reduction of $[M(CO)_4(N,N)]$ at room temperature in *n*PrCN solutions. The band intensities did not change with time and the parent spectra were recovered by re-oxidation at more positive potentials, confirming the chemical stability of $[M(CO)_4(N,N)]^{\bullet -}$. The IR spectral patterns of the radical anions and the parent neutral complexes are identical (see ESI), demonstrating their close structural similarity. The wavenumbers of the ν(CO) IR bands are listed in Table 1. The shift to lower wavenumbers upon reduction is caused by a shift of electron density toward the CO ligands.[40,42] Depending on the particular vibration, the magnitude of this shift is 2–10 cm^{-1} smaller for tmp than phen complexes.

UV-Vis spectroelectrochemistry. The UV-Vis spectra monitored in the course of an electrochemical reduction of $[M(CO)_4(N,N)]$ in THF solution show an isosbestic conversion of the $[M(CO)_4(N,N)]$ spectral pattern into that characteristic of $phen^{\bullet -}$ or $tmp^{\bullet -}$ radical anions, confirming the localization of the reduction on the N,N ligand. These spectra are rather similar for all four reduced complexes. They show a strong band at 400–420 nm and a structured absorption band between 550 and 650 nm, which extends into the red (or even NIR) spectral region, see the ESI.

DFT calculations. DFT calculations were performed on all four radical anionic $[M(CO)_4(N,N)]^{\bullet -}$ complexes in order to optimize their molecular geometries, understand their electronic structures and interpret the EPR spectra. The electronic ground states of $[M(CO)_4(phen)]^{\bullet -}$ and $[M(CO)_4(tmp)]^{\bullet -}$ were identified as $^2B_1$ and $^2A_2$, respectively, regardless of the metal atom: Cr or W. Accordingly, the unpaired electron occupies the SOMO which has b_1 symmetry for the phen complexes and a_2 for their tmp counterparts. The molecular orbital ordering shown in Fig. 2 is valid also for the radical anions $[M(CO)_4(N,N)]^{\bullet -}$. The composition of the relevant molecular orbitals (Table 2) is, within 2%, the same for the neutral complexes and the corresponding radical anions. The calculated bond length changes due to reduction are different for the phen and tmp complexes (ESI). They reflect the bonding and antibonding characters with respect to individual intraligand bonds of the respective SOMOs, Fig. 3.

EPR spectra of $[M(CO)_4(N,N)]^{\bullet -}$. Table 5 lists hyperfine splitting (hfs) constants calculated for each radical anionic complex assuming the $^2B_1$ as well as $^2A_2$ ground state. The predicted EPR patterns are distinctively different. The $^2B_1$ state is characterized by a large hfs from the nitrogen donor atoms and from two pairs of hydrogen atoms bound at the C3,8 and C4,7 positions. On the other hand, the $^2A_2$ state is predicted to show a small nitrogen hfs and large hfs from pairs of hydrogen atoms at the positions C2,9, C4,7 and C5,6. If any of these positions bears a CH_3 group, large hfs are predicted for the corresponding methyl protons. Hyperfine splitting from metal atoms was calculated to be generally low, but much larger for the $^2B_1$ than $^2A_2$ state.

Experimental EPR spectra of electrogenerated radical anions (Fig. 6) were obtained for all four $[M(CO)_4(N,N)]$ complexes at room temperature in *n*PrCN. For $[Cr(CO)_4(tmp)]$ the measurement was performed at −90 °C in order to get sufficient spectral resolution. The spectra are typical for metal complexes with radical ligands.[56] The *g* factors (Table 5) are slightly larger than the "free" ligand values:[8] 2.0027 for $tmp^{\bullet -}$ and 2.0030 for $phen^{\bullet -}$. The experimental hyperfine splitting (hfs) constants were determined by computer fitting. They

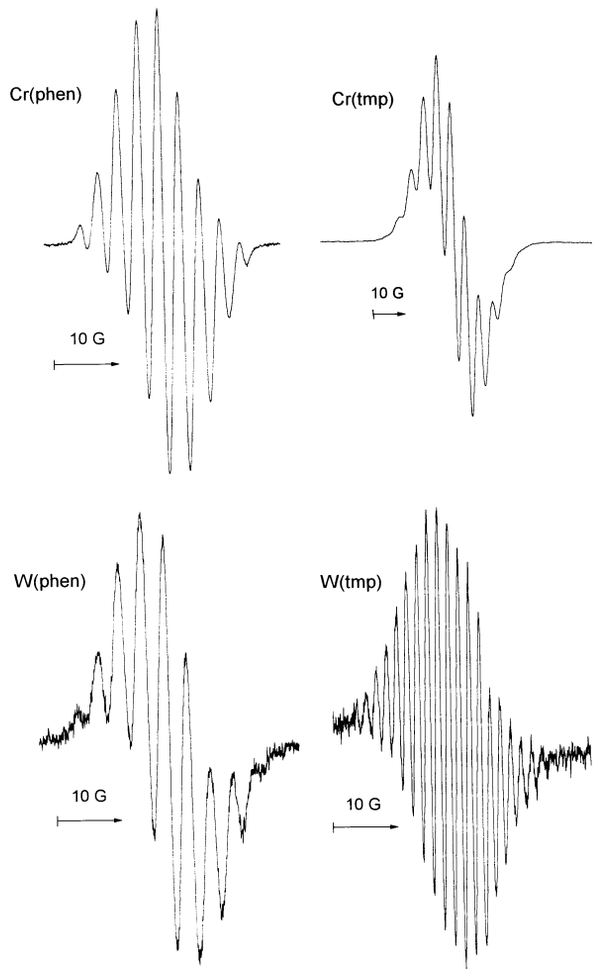

Fig. 6 EPR spectra of electrochemically generated $[M(CO)_4(N,N)]^{\bullet -}$ radical anions (M = Cr or W; N,N = phen or tmp). Measured in THF at room temperature with the exception of $[Cr(CO)_4(tmp)]^{\bullet -}$: −90 °C, *n*PrCN.

are listed in Table 5. For each complex, two different fits were performed, using starting sets of hfs constants corresponding to a $^2A_2$ and $^2B_1$ ground state, respectively. The starting sets were estimated from the DFT-calculated values (Table 5) and from the hfs of free[8] $phen^{\bullet -}$ and $tmp^{\bullet -}$. It followed that EPR spectra of $[M(CO)_4(phen)]^{\bullet -}$; M = Cr or W, can be fitted only to the set of parameters typical for a $^2B_1$ state. The spectra show large hfs from a pair of nitrogen atoms and from the two pairs of protons bound at C3,8 and C4,7. On the other hand, EPR spectra of $[M(CO)_4(tmp)]^{\bullet -}$, M = Cr or W, can be computer-fitted only under the assumption of an $^2A_2$ ground state. The spectra show large hfs from the C2,9 pair of ^1H nuclei and from six protons of one pair of CH_3 groups bound at C4,7 positions. A moderate hfs due to ^1H atoms at C5,6 positions and small nitrogen hfs also contribute. Metal (^{53}Cr-(9.54%), ^{183}W(14.28%)) hfs is not apparent in any of the spectra measured, due to insufficient resolution.

A reasonable qualitative agreement between experimental and calculated hfs constants was achieved (Table 5). The respective sets of EPR parameters corresponding to the $^2A_2$ and $^2B_1$ states are sufficiently different to allow for an unequivocal assignment of the ground state : $^2B_1$ for $[M(CO)_4(phen)]^{\bullet -}$ and $^2A_2$ for $[M(CO)_4(tmp)]^{\bullet -}$, M = Cr or W. It is expected that this criterion can be used also for other radical-anionic complexes of phen-type ligands.

Discussion

The energetic order of the two lowest-lying unoccupied π* orbitals (b_1, a_2) of the N,N ligand in $[M(CO)_4(N,N)]$, M = Cr or W; N,N = phen or tmp, changes on methylation of the phen ligand from $a_2 > b_1$ to $b_1 > a_2$. This means that phen and tmp complexes have different LUMOs: b_1 and a_2, respectively. Although these two orbitals are close in energy and both are predominantly N,N ligand-localized, their distributions over the N,N ligand and the $M(CO)_4$ fragment are very different, Fig. 3. The b_1 orbital is partly delocalized over $M(CO)_4$ *via* overlap with the d_{xz} orbital and the σ–π* interaction[42] with the axial OC–M–CO moiety. On the other hand, the a_2 orbital is nearly purely ligand-localized, virtually unable to accept any electron density from the $M(CO)_4$ fragment. Nevertheless, the effects of b_1/a_2 LUMO switching on the properties of neutral $[M(CO)_4(N,N)]$ complexes are very small. The b_1(LUMO + 1) of the tmp complexes is a low-lying orbital which is still involved in a M→N,N π-back bonding, albeit to a slightly smaller extent than for phen, see Table 2. Consequently, the *ν*(CO) vibrational frequencies are only a little lower for tmp than phen complexes.

Importantly, the visible absorption, resonance Raman and luminescence spectra of phen and tmp complexes are very similar. Switching of the energetic order of the lowest unoccupied b_1 and a_2 orbitals has no effect on the character and energy order of the electronic transitions which give rise to the visible MLCT absorption band, except for small changes in the relative importance of the contributing orbital excitations. This is because the principal contributor is not the HOMO ⟶ LUMO transition but the a $^1A_1 \longrightarrow b^1A_1$ transition which is dominated by excitation between the metal and ligand orbitals of b_1 symmetry which overlap well, whether the b_1(phen or tmp) orbital is the LUMO or not. Moreover, the transition energies are not simply the differences in energies of the orbitals involved in the excitations. The LUMO switching thus does not affect the energetic order of the transitions which contribute to the optical absorption. The larger solvatochromism and relative resonance enhancement of the *ν*(CO) A_1^2 Raman peak observed for tmp are due to the higher localization of the b_1(HOMO) and b_1(LUMO or LUMO + 1) orbitals at the $M(CO)_4$ and N,N moieties.

By contrast with the neutral complexes, the differences

Table 5 Observed and calculated EPR parameters, measured in THF at room temperature with the exception of $[Cr(CO)_4(tmp)]^{\bullet -}$: −90 °C, *n*PrCN.

	Experimental splitting			DFT[a] (10^{-4} cm^{-1})	
Compound	G		10^{-4} cm^{-1}	$^2B_1$	$^2A_2$
$[Cr(CO)_4(phen)]$	*a*(Cr)	—	—	0.57	(0.21)
g = 2.0022	*a*(N)	3.68	3.44	4.72	(0.59)
	a(H2)	—	—	0.21	(−5.51)
	a(H3)	3.08	2.88	3.86	(0.85)
	a(H4)	2.78	2.60	2.65	(−4.37)
	a(H5)	—		0.05	(−3.83)
$[Cr(CO)_4(tmp)]$	*a*(Cr)	—	—	(0.65)	0.18
g = 2.0044	*a*(N)	0.88	0.82	(4.71)	0.52
	a(H2)	3.86	3.61	(0.06)	4.86
	a(H3*)	0.08	0.07	(4.01)	0.90
	a(H4*)	3.88	3.63	(2.77)	3.88
	a(H5)	3.39	3.17	(0.02)	3.85
$[W(CO)_4(phen)]$	*a*(W)	—	—	−2.54	(−0.10)
g = 2.0049	*a*(N)	3.23	3.02	4.59	(0.51)
	a(H2)	—	—	0.06	(−5.87)
	a(H3)	4.06	3.80	−3.80	(0.95)
	a(H4)	2.90	2.71	−2.88	(−4.79)
	a(H5)	—	—	−0.05	(−3.98)
$[W(CO)_4(tmp)]$	*a*(W)	—	—	(−2.43)	−0.09
g = 2.0049	*a*(N)	0.25	0.23	(4.50)	0.42
	a(H2)	4.54	4.25	(−0.06)	−5.31
	a(H3*)	—	—	(3.77)	0.93
	a(H4*)	3.25	3.04	(2.83)	4.11
	a(H5)	1.71	1.60	(0.02)	−4.02

Methyl protons are asterisked. [a]Splitting constants calculated for the wrong ground state are shown in parentheses.

between phen and tmp complexes caused by the b_1/a_2 LUMO switching become prominent upon reduction to radical anions $[M(CO)_4(N,N)]^{\bullet -}$. Now, the b_1 and a_2 orbitals are singly occupied for N,N = phen and tmp, respectively. Hence, radical anionic phen and tmp complexes have different respective ground states, $^2B_1$ and $^2A_2$, with very different molecular structures and unpaired electron density distribution. This is especially evident from the EPR spectra, which show completely different hfs splitting patterns for phen and tmp complexes (Table 5).

Further differences were observed in IR spectroelectrochemistry which shows a smaller decrease of ν(CO) frequencies on reduction for tmp complexes than those of phen. Moreover, the difference between the reduction potentials of the complexes and of the corresponding "free" ligands[8] are 40 (Cr) and 90 mV (W) larger for phen than tmp. Both these effects are caused by the larger delocalization of electron density from the reduced $phen^{\bullet -}$ ligand to the $M(CO)_4$ moiety.

The change of the LUMO of 1,10-phenathroline complexes from b_1 to a_2 is caused by placing electron-donating Me substituents at the C(3,8) positions where the b_1 orbital, but not a_2, is heavily localized, see Figs. 1 and 3. One can expect the same orbital switching upon attaching electron accepting groups at the C(5,6) or C(2,9) positions, stabilizing a_2 relative to b_1. However, this hypothesis was not tested experimentally. By contrast, the localization of both the b_1 and a_2 orbitals at C(4,7) is similar. Hence, substitutents at these positions do not lead to a LUMO switching. Accordingly, 4,7-Me_2-phen has a $^2B_1$ ground state.[7,8]

In principle, LUMO switching could take place when phen-type molecular fragments are incorporated into a supramolecular system. Based on the results discussed above, it can be expected that b_1/a_2 LUMO switching would be of little relevance when building photonic molecular devices. On the other hand, large effects are expected should a phen-containing moiety be incorporated into redox switches or molecular wires.

Acknowledgements

This work is part of an European collaboration COST Action D14, project D14/0001/99. The COST Short Term Scientific Mission programme is acknowledged for financing the stays of I. R. Farrell at the Universiteit van Amsterdam and at the J. Heyrovský Institute, Prague. Financial support was provided by grant no. OC.D14.20 (Ministry of Education, Czech Republic), QMW College, London and by the Central Research Fund, University of London. Mr C. P. Groen is thanked for his help with measurements of resonance Raman spectra. Stimulating discussions with Professor D. J. Stufkens are gratefully appreciated.

References

1 D. J. Stufkens, *Coord. Chem. Rev.*, 1990, **104**, 39.
2 A. Vlček, Jr., in *Electron Transfer in Chemistry*, Vol. 2, ed. D. Astruc, Wiley-VCH, Weinheim, 2001, p. 804.
3 A. Juris, V. Balzani, F. Barigelletti, S. Campagna, P. Belser and A. von Zelewsky, *Coord. Chem. Rev.*, 1988, **84**, 85.
4 D. J. Stufkens and A. Vlček, Jr., *Coord. Chem. Rev.*, 1998, **177**, 127.
5 W. Kaim and S. Ernst, *J. Phys. Chem.*, 1986, **90**, 5010.
6 A. Klein, C. Vogler and W. Kaim, *Organometallics*, 1996, **15**, 236.
7 W. Kaim, *J. Am. Chem. Soc.*, 1982, **104**, 3883.
8 A. Klein, W. Kaim, E. Waldhör and H.-D. Hausen, *J. Chem. Soc., Perkin Trans. 2*, 1995, 2121.
9 S. Ernst, C. Vogler, A. Klein, W. Kaim and S. Záliš, *Inorg. Chem.*, 1996, **35**, 1295.
10 R. Ziessel, *J. Chem. Soc., Chem. Commun.*, 1988, 16.
11 R. Ziessel, *Angew. Chem., Int. Ed. Engl.*, 1991, **30**, 844.
12 A. Juris, L. Prodi, A. Harriman, R. Ziessel, M. Hissler, A. El-ghayoury, F. Wu, E. C. Riesgo and R. P. Thummel, *Inorg. Chem.*, 2000, **39**, 3590.
13 L. S. Kelso, T. A. Smith, A. C. Schultz, P. C. Junk, R. N. Warrener, K. P. Ghiggino and F. R. Keene, *J. Chem. Soc., Dalton Trans.*, 2000, 2599.
14 C. Dietrich-Buchecker, J.-P. Sauvage and J.-M. Kern, *J. Am. Chem. Soc.*, 1989, **111**, 7791.
15 N. Armaroli, F. Diederich, C. O. Dietrich-Buchecker, L. Flamigni, J.-F. Nierengarten and J.-P. Sauvage, *Chem. Eur. J.*, 1998, **4**, 406.
16 J.-M. Kern, J.-P. Sauvage, J.-L. Weidmann, N. Armaroli, L. Flamigni, P. Ceroni and V. Balzani, *Inorg. Chem.*, 1997, **36**, 5329.
17 J.-C. Chambron, J.-P. Collin, J.-O. Dalbavie, C. O. Dietrich-Buchecker, V. Heitz, F. Odobel, N. Solladié and J.-P. Sauvage, *Coord. Chem. Rev.*, 1998, **178**–**180**, 1299.
18 D. S. Tyson and F. N. Castellano, *Inorg. Chem.*, 1999, **38**, 4382.
19 H. S. Joshi, R. Jamshidi and Y. Tor, *Angew. Chem., Int. Ed.*, 1999, **38**, 2722.
20 P. G. Sammes and G. Yahioglu, *Chem. Soc. Rev.*, 1994, **23**, 327.
21 J. K. Barton, in *Bioinorganic Chemistry*, eds. I. Bertini, H. B. Gray, S. J. Lippard and J. S. Valentine, University Science Books, Mill Valley, CA, 1994.
22 L. Wallace and D. P. Rillema, *Inorg. Chem.*, 1993, **32**, 3836.
23 L. Wallace, D. C. Jackman, D. P. Rillema and J. W. Merkert, *Inorg. Chem.*, 1995, **34**, 5210.
24 L. Sacksteder, M. Lee, J. N. Demas and B. A. DeGraff, *J. Am. Chem. Soc.*, 1993, **115**, 8230.
25 P. Federlin, J.-M. Kern, A. Rastegar, C. Dietrich-Buchecker, P. A. Marnot and J.-P. Sauvage, *New. J. Chem.*, 1990, **14**, 9.
26 E. J. Baerends, A. Bérces, C. Bo, P. M. Boerrigter, L. Cavallo, L. Deng, R. M. Dickson, D. E. Ellis, L. Fan, T. H. Fischer, C. Fonseca Guerra, S. J. A. van Gisbergen, J. A. Groeneveld, O. V. Gritsenko, F. E. Harris, P. van den Hoek, H. Jacobsen, G. van Kessel, F. Kootstra, E. van Lenthe, V. P. Osinga, P. H. T. Philipsen, D. Post, C. C. Pye, W. Ravenek, P. Ros, P. R. T. Schipper, G. Schreckenbach, J. G. Snijders, M. Sola, D. Swerhone, G. te Velde, P. Vernooijs, L. Versluis, O. Visser, E. van Wezenbeek, G. Wiesenekker, S. K. Wolff, T. K. Woo and T. Ziegler, ADF 1999.01, Amsterdam, 1999.
27 C. Fonseca Guerra, J. G. Snijders, G. te Velde and E. J. Baerends, *Theor. Chim. Acta*, 1998, **99**, 391.
28 S. J. A. van Gisbergen, J. G. Snijders and E. J. Baerends, *Comput. Phys. Commun.*, 1999, **118**, 119.
29 A. D. Becke, *Phys. Rev. A*, 1988, **38**, 3098.
30 J. P. Perdew, *Phys. Rev. A*, 1986, **33**, 8822.
31 M. H. B. Stiddard, *J. Chem. Soc.*, 1962, 4712.
32 A. M. Bond, K. B. Oldham and G. A. Snook, *Anal. Chem.*, 2000, **72**, 3492.
33 M. Krejčík, M. Daněk and F. Hartl, *J. Electroanal. Chem., Interfacial Electrochem.*, 1991, **317**, 179.
34 F. Hartl, R. P. Groenestein and T. Mahabiersing, *Coll. Czech. Chem. Commun.*, in press.
35 B. Hutchinson and K. Nakamoto, *Inorg. Chim. Acta*, 1969, **3**, 591.
36 L. E. Orgel, *Inorg. Chem.*, 1962, **1**, 25.
37 R. T. Jernigan, R. A. Brown and G. R. Dobson, *J. Coord. Chem.*, 1972, **2**, 47.
38 C. S. Kraihanzel and F. A. Cotton, *Inorg. Chem.*, 1963, **2**, 533.
39 F. A. Cotton and C. S. Kraihanzel, *J. Am. Chem. Soc.*, 1962, **84**, 4432.
40 A. Vlček, Jr., F. Baumann, W. Kaim, F.-W. Grevels and F. Hartl, *J. Chem. Soc., Dalton Trans.*, 1998, 215.
41 A. Vlček, Jr., F.-W. Grevels, T. L. Snoeck and D. J. Stufkens, *Inorg. Chim. Acta*, 1998, **278**, 83.
42 S. Záliš, C. Daniel and A. Vlček, Jr., *J. Chem. Soc., Dalton Trans.*, 1999, 3081.
43 H. Jinshuan, C. Qingrong, W. Manfrag and H. Meiyun, *Chin. J. Struct. Chem.*, 1985, **4**, 66.
44 N. S. Magomedova and G. K.-I. Magomedov, *Metalloorg. Khim.*, 1990, **3**, 129.
45 H. Jinshuan, C. Qingrong, W. Manfrag and L. Shimei, *Chin. J. Struct. Chem.*, 1985, **4**, 69.
46 P. C. Servaas, H. K. van Dijk, T. L. Snoeck, D. J. Stufkens and A. Oskam, *Inorg. Chem.*, 1985, **24**, 4494.
47 R. W. Balk, T. L. Snoeck, D. J. Stufkens and A. Oskam, *Inorg. Chem.*, 1980, **19**, 3015.
48 K. A. Rawlins and A. J. Lees, *Inorg. Chem.*, 1989, **28**, 2154.
49 D. M. Manuta and A. J. Lees, *Inorg. Chem.*, 1986, **25**, 1354.
50 H. Saito, J. Fujita and K. Saito, *Bull. Chem. Soc. Jpn.*, 1968, **41**, 359.
51 H. Saito, J. Fujita and K. Saito, *Bull. Chem. Soc. Jpn.*, 1968, **41**, 863.
52 R. W. Balk, D. J. Stufkens and A. Oskam, *Inorg. Chim. Acta*, 1979, **34**, 267.
53 C. Pollak, A. Rosa and E. J. Baerends, *J. Am. Chem. Soc.*, 1997, **119**, 7324.
54 A. Rosa, E. J. Baerends, S. J. A. van Gisbergen, E. van Lenthe, J. A. Groeneveld and J. G. Snijders, *J. Am. Chem. Soc.*, 1999, **121**, 10356.
55 Y. J. Chang, X. Xu, T. Yabe, S.-C. Yu, D. R. Anderson, L. K. Orman and J. B. Hopkins, *J. Phys. Chem.*, 1990, **94**, 729.
56 W. Kaim, *Coord. Chem. Rev.*, 1987, **76**, 187.